8 Vehicle stability

8.1 Effective cornering stiffness

In the previous chapter it was established that all modern cars are understeer, and that the effective front cornering stiffness, C_{12}, is considerably lower than the corresponding value rear, C_{34}. This might seem strange, since typically the front and rear wheels are of the same type, with essentially the same air pressure and load. The explanation is that the tyre and wheel can not be seen as an isolated component, but a as a part that interacts with the rest of the suspension. Some of the most important factors are:

1. A nonzero angle between the wheel plane and the ground, which is determined by the suspension, induces lateral forces called *camber forces*.

2. The wheel suspension and the steering system contain elastic elements which gives a reduction in the effective cornering stiffness.

3. Steering angle changes caused by the suspension kinematics.

4. The sensitivity of the tyres to vertical loads.

These factors will in the following be studied in detailed and combined into a linear model where the size of the respective factor can be estimated.

8.2 Camber

If a wheel, which is rolling straight ahead, is leaned an angle γ to the side, a reaction force results due to the imposed straight motion. This happens since the wheel strives to roll like a cone, with its tip at the point where the axle of rotation intersects the ground plane. The direction of the reaction force is intuitively seen from figure 8.2-1. In a neighbourhood of a given load, the camber force can be assumed to be proportional to the normal force and camber angle. Note that it is the angle to the ground surface normal which is decisive.

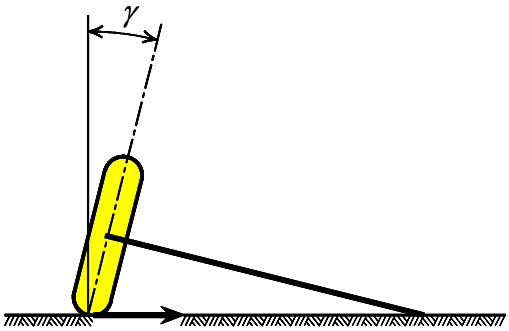

Figure 8.2-1 Rolling wheel with the direction of the reaction force due to a camber angle with respect to ground γ.

This can be used to change the understeer gradient of a vehicle. The wheels can be adjusted such that they get a static camber angle ε_0, which is usually defined positive if the wheel leans outward from the car body, see figure 8.2-2. Note that camber angles with respect to the car body will be denoted ε and with respect to the ground γ.

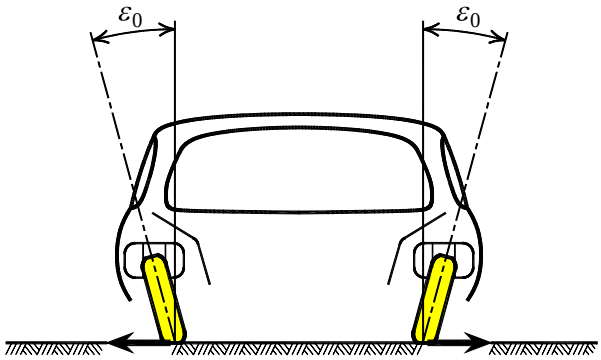

Figure 8.2-2 Positive direction for static camber angles as defined when setting up wheel suspensions.

The wheels on the same axle generate opposing forces which cancel each other when driving straight ahead. At cornering, there will be a load transfer from the curve-inner to the curve-outer wheel. Since the camber force is approximately proportional to the normal force, a corresponding change of the camber force occurs, as shown in figures 8.2-3 and 8.2-4.

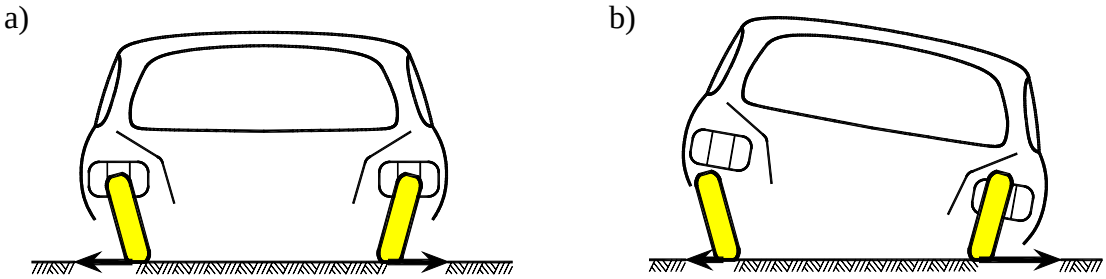

Figure 8.2-3 Influence of positive static camber at cornering. View from behind.

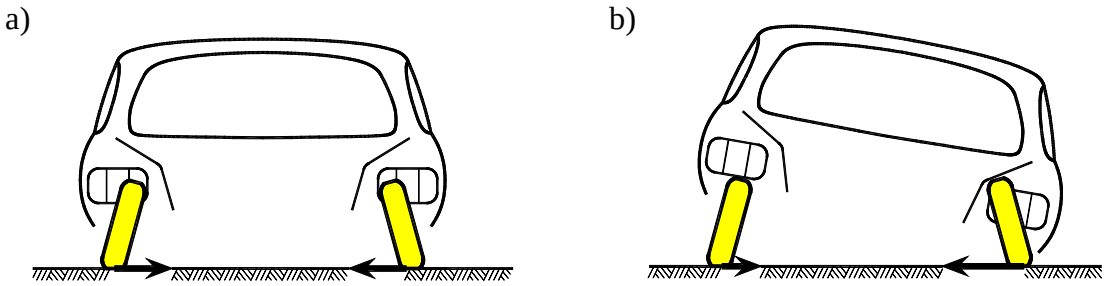

Figure 8.2-4 Influence of negative static camber at cornering. View from behind.

If 8.2-3 is the front axle and 8.2-4 is the rear axle, both axles contribute toward the understeer direction. Conversely, positive static camber on the rear axle and negative static camber on the front axle both contribute toward the oversteer direction.

Decisive for the magnitude of the camber force is the wheel's angle relative to the ground surface normal, and not the angle relative to the car body. Consider the simple case that the wheels move parallel to the car body at compression (jounce) and expansion (rebound) of the suspension. At cornering, the wheels will attain a camber angle to the ground plane due to roll of the car body, see figure 8.2-5.

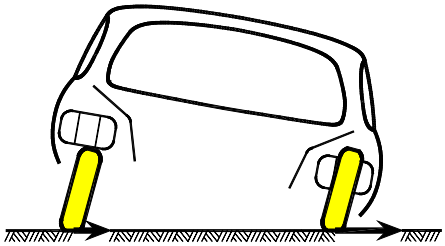

Figure 8.2-5 Influence of camber due to roll at cornering. View from behind.

Normally, the angle of the wheels relative to the car body will vary when the suspension is compressed or expanded. Depending on the construction of the wheel suspension, i.e. the position of the centre of rotation the camber angle change will vary. Two examples are given in figures 8.2-6 and 8.2-7.

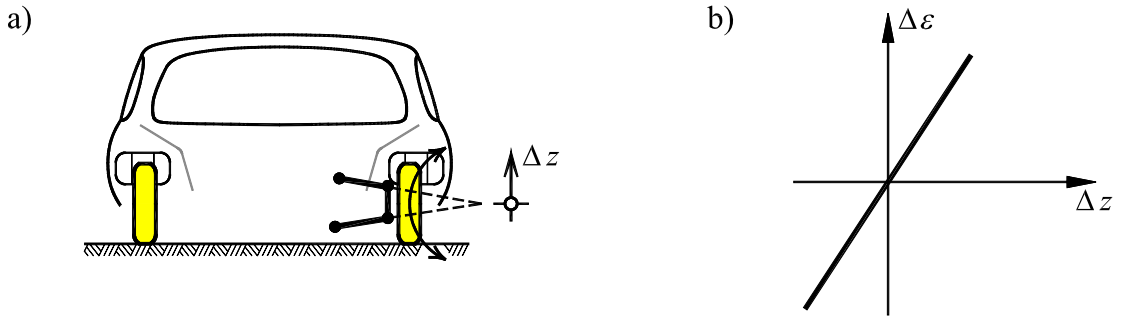

Figure 8.2-6 Camber change at jounce and rebound for a suspension with its centre of rotation towards the outside of the car body.

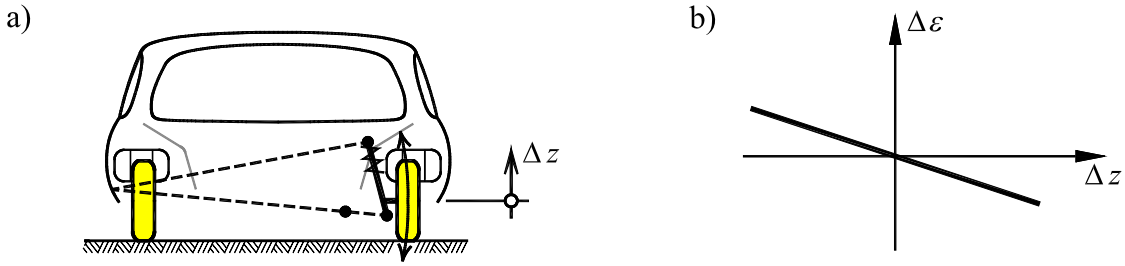

Figure 8.2-7 Camber change at jounce and rebound for a suspension with its centre of rotation towards the inside of the car body.

In reality, a diagram which describes the camber angle relative to the car body as a function of compression and expansion distance of a McPherson suspension will look like in figure 8.2-8.

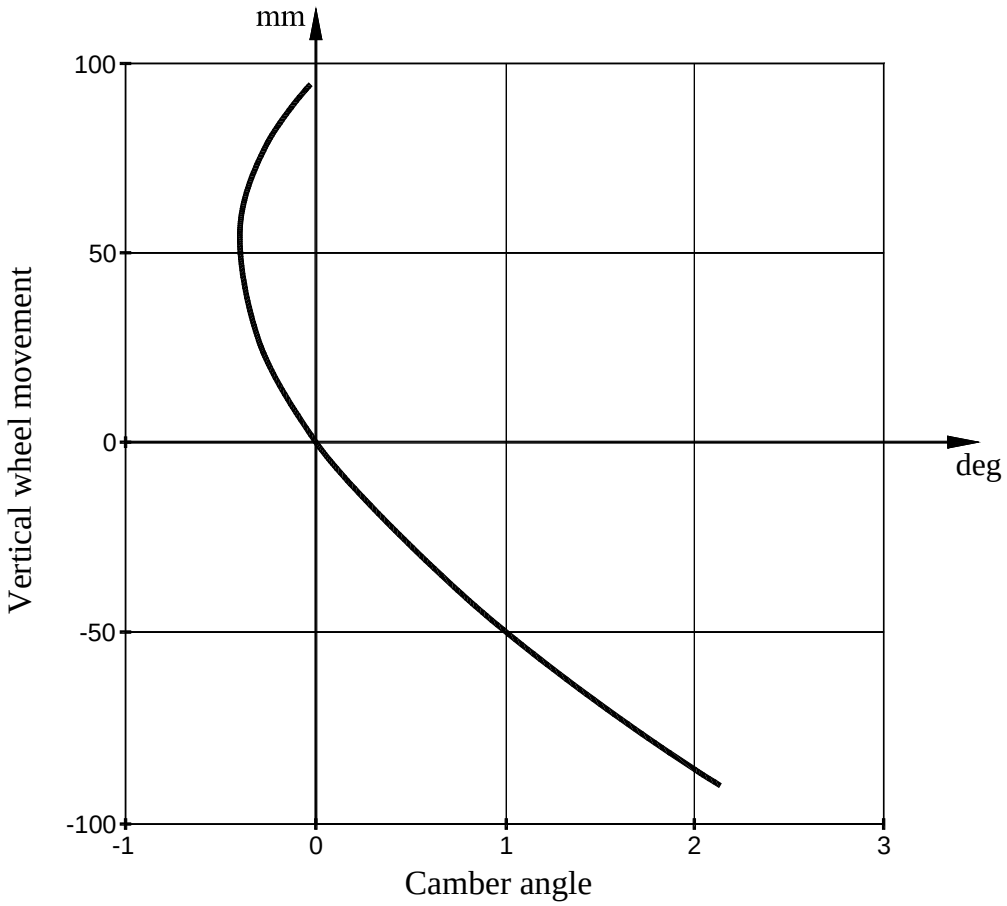

Figure 8.2-8 Change in camber angle to car body, at jounce and rebound of a McPherson front suspension.

At cornering, the suspension of the curve-outer wheel will be compressed ($\Delta z > 0$) and for the curve-inner wheel be expanded ($\Delta z < 0$). If the camber change at compression and expansion is approximated as linear the corresponding camber angles relative to the car body are:

$$\varepsilon_{co} = \frac{\partial \varepsilon}{\partial z} \cdot \Delta z_o ; \varepsilon_{ci} = \frac{\partial \varepsilon}{\partial z} \cdot \Delta z_i$$

$$\Delta z_o = \Delta S ; \Delta z_i = -\Delta S$$

where a subscript '*o*' denotes outer and '*i*' inner wheel. Consider a roll angle $\phi > 0$. If the track width is denoted *b*, the suspension displacement is to linear order

$$\Delta S = \frac{b}{2} \cdot \phi$$

Define the camber angle relative to ground, γ, to have positive direction according to the right hand rule. γ is composed of the roll angle, ϕ, and the camber angle relative to the car body ε. For the curve-inner wheel it follows that

$$\gamma_i = \phi - \varepsilon_i = \phi - \frac{\partial \varepsilon}{\partial z} \cdot (-\frac{b}{2} \cdot \phi) = \phi \left(1 + \frac{b}{2} \cdot \frac{\partial \varepsilon}{\partial z} \right)$$

and in the corresponding way for the curve-outer wheel

$$\gamma_o = \phi + \varepsilon_o = \phi + \frac{\partial \varepsilon}{\partial z} \cdot \frac{b}{2} \cdot \phi = \phi \left(1 + \frac{b}{2} \cdot \frac{\partial \varepsilon}{\partial z} \right)$$

It thus follows that

$$\frac{\partial \gamma_{o,i}}{\partial \phi} = 1 + \frac{b}{2} \cdot \frac{\partial \varepsilon}{\partial z} \qquad (8.2.1)$$

i.e. exactly the same expression for both curve-inner and curve-outer wheel if $\gamma_{o,i}$ have the same positive direction (according to the right hand rule). This means that for small roll angles, the camber forces of both wheels on an axle are in the same direction. Naturally, a similar analysis shows that equation (8.2.1) is also true for negative roll angles, $\phi < 0$, although intermediate steps differ slightly.

It thus follows for the respective axle:

$$\text{Front axle}: \frac{\partial \gamma}{\partial \phi} = \begin{cases} > 0 & \text{understeer} \\ < 0 & \text{oversteer} \end{cases}$$

$$\text{Rear axle}: \frac{\partial \gamma}{\partial \phi} = \begin{cases} > 0 & \text{oversteer} \\ < 0 & \text{understeer} \end{cases}$$

Linearization around the origin in figure 8.2-8 yields

$$\frac{\partial \varepsilon}{\partial z} \approx -\frac{\frac{1 \cdot \pi}{180}}{0{,}050} \approx -0{,}35$$

and substitution of b = 1.45 m gives

$$\frac{\partial \gamma}{\partial \phi} \approx 1 + \frac{1{,}45}{2} \cdot (-0{,}35) \approx 0{,}75$$

which is a realistic value.

If the camber force F_γ for a wheel is positive in the direction of the y-axis, as defined in figure 1.3-1, and γ has a positive direction according to the right hand rule, then

$$F_\gamma = -C_\gamma \cdot \gamma$$

where C_γ is called the camber stiffness (the minus sign is introduced for C_γ to be positive). In a neighbourhood of a certain load condition, C_γ can be assumed to be proportional to the normal force and the air pressure in the tyre, but the different gradients are very different for different types of tyres and brands.

In theoretical analyses the camber force can be modelled as a shift in the lateral force curve by assuming that the camber angle, γ, is assumed to correspond to a slip angle, α_γ, through the relationship

$$F_\gamma = -C_\gamma \cdot \gamma = -C_\alpha \cdot \alpha_\gamma$$

$$\alpha_\gamma = \frac{C_\gamma}{C_\alpha} \cdot \gamma$$

The resulting lateral force is therefore

$$-\left(F_y + F_\gamma\right) = C_\alpha \cdot (\alpha + \alpha_\gamma)$$

This is schematically shown in figure 8.2-9.

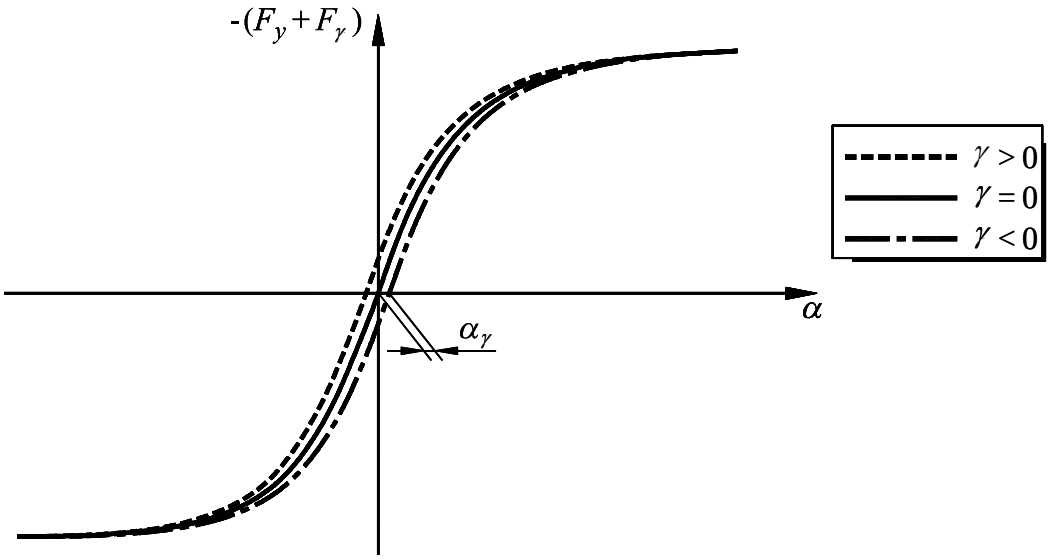

Figure 8.2-9 Resulting lateral force as a function of slip angle and camber angle.

The dependence of the camber force on the camber angle, γ, can also be replaced by applying the following equivalent steer angle, δ_γ,

$$\delta_\gamma = -\alpha_\gamma = -\frac{C_\gamma}{C_\alpha} \cdot \gamma \qquad (8.2.2)$$

This will later be used.

8.3 Elastic elements in the wheel suspension

Through linkage and elastic elements (rubber bushings) the effective cornering stiffness can be altered compared to the cornering stiffness of the wheel alone. To enlighten this fact, consider the simplified front wheel suspension in figure 8.3-1.

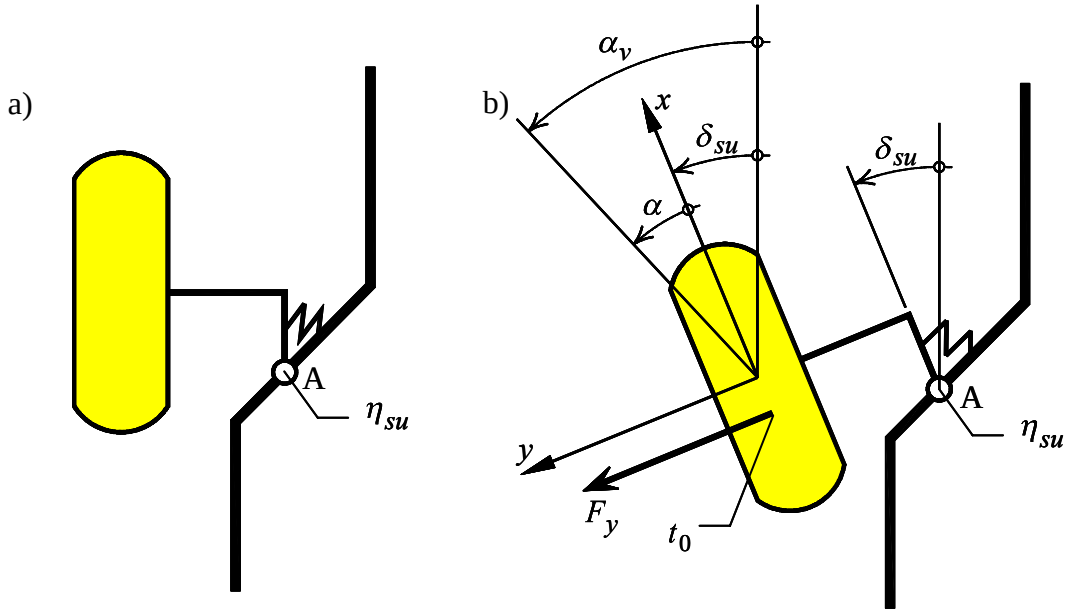

Figure 8.3-1 Influence of elastic suspension
a) straight ahead driving
b) circular driving to the left

In the figure it is shown that F_y develops a certain distance behind the centre of the tyre. This causes the force to exert a torque on the wheel called the *aligning moment*. The offset distance of the force from the centre of the tyre is called the pneumatic trail, t_0:

$$t_0 = \left(\frac{M_z}{F_y} \right)_{\alpha=0}$$

It follows that $$F_y(n_{su} - t_0) = -C_{su} \cdot \delta_{su} \qquad (8.3.1)$$

where C_{su} is the torsion stiffness around A, n_{su} and t_0 are x-coordinates in the tyre frame and δ_{su} is the contribution to the steer angle from the compliance in the suspension.

Furthermore, $$F_y = -C_\alpha \cdot \alpha = -C_{\alpha v} \cdot \alpha_v \qquad (8.3.2)$$

where $C_{\alpha v}$ = effective cornering stiffness (for one side)
α_v = slip angle of the vehicle

However, $$\alpha_v = \delta_{su} + \alpha \qquad (8.3.3)$$

Substitution of (8.3.1) and (8.3.2) into (8.3.3) yields

$$\frac{1}{C_{\alpha v}} = \frac{1}{C_\alpha} + \frac{n_{su} - t_0}{C_{su}}$$

If the reaction point A is behind the acting point of the lateral force, i.e. $n_{su} - t_0 < 0$, then the result is an increased effective cornering stiffness, i.e. $C_{\alpha v} > C_\alpha$.

Conversely, it follows that $C_{\alpha v} < C_\alpha$ if $n_{su} - t_0 > 0$.

This was valid for one side, and in total for one axle it follows that

$$C_{\alpha T} = \frac{2}{\frac{1}{C_\alpha} + \frac{n_{su} - t_0}{C_{su}}}$$

where $C_{\alpha T}$ is the effective cornering stiffness for the axle.

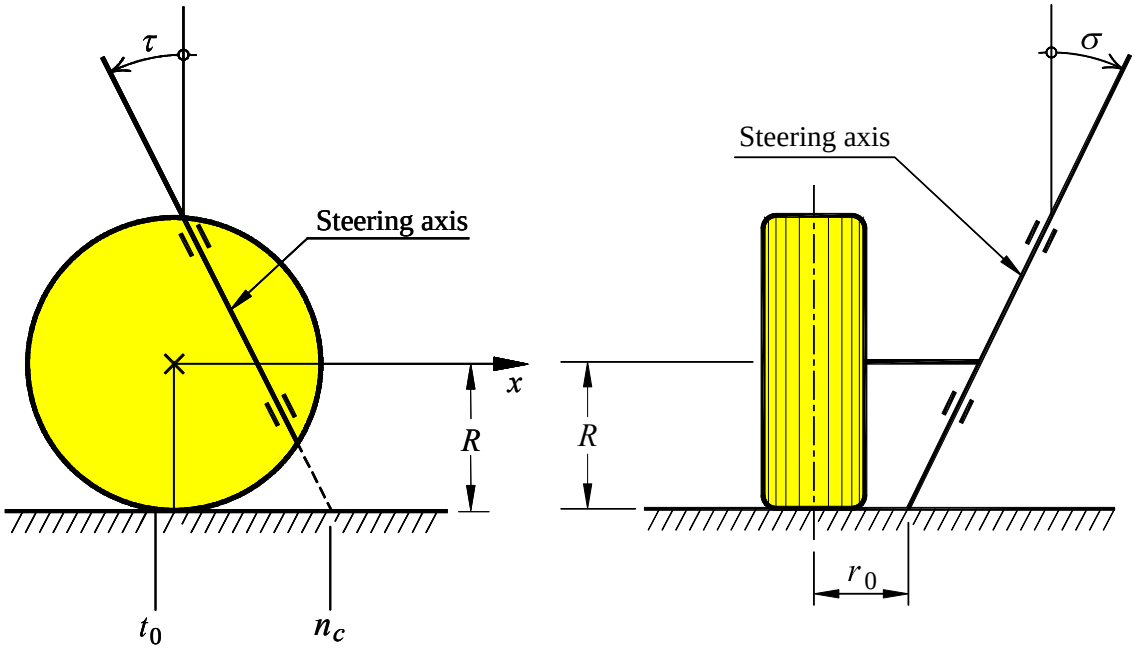

Figure 8.3-2 *Front wheel viewed from the side and from behind*

τ = caster *angle*
n_c = *caster distance*
t_0 = *pneumatic trail*
σ = *kingpin inclination angle*
r_0 = *kingpin offset at ground*

For the front axle the steering system itself has a compliance which affects the effective cornering stiffness. Consider a rack and pinion steering system, and assume that all elasticity is in the steering shaft (C_s Nm / rad). If the steering ratio is i_s the stiffness at the wheel is reduced to

$$C_s' = i_s^2 \cdot C_s$$

This is the stiffness around the steering axis. With notation according to figure 8.3-2 it follows that

$$2 \cdot F_y \cdot (n_c - t_0) = -C_s' \cdot \delta_s'$$

where δ_s' is the contribution to the steering angle due to steering elasticity, and n_c and t_0 are *x*-coordinates in the tyre fixed coordinate system.

Thus,

$$\delta_s' = -\frac{2(n_c - t_0)}{C_s'} \cdot F_y$$

and this added to equation (8.3.3) yields

$$C_{\alpha T} = \frac{2}{\frac{1}{C_\alpha} + \frac{n_{su} - t_0}{C_{su}} + \frac{2(n_c - t_0)}{C_s'}} \qquad (8.3.4)$$

8.4 Roll steer and suspension kinematics

At cornering, the curve-outer wheel is more heavily loaded and in jounce, while the curve-inner wheel is unloaded and in rebound. It is very common that the wheel does not move parallel with the car body, but steers inwards (toe in) or outwards (toe out). Figure 8.4-1 shows the angle change for a typical McPherson-suspension.

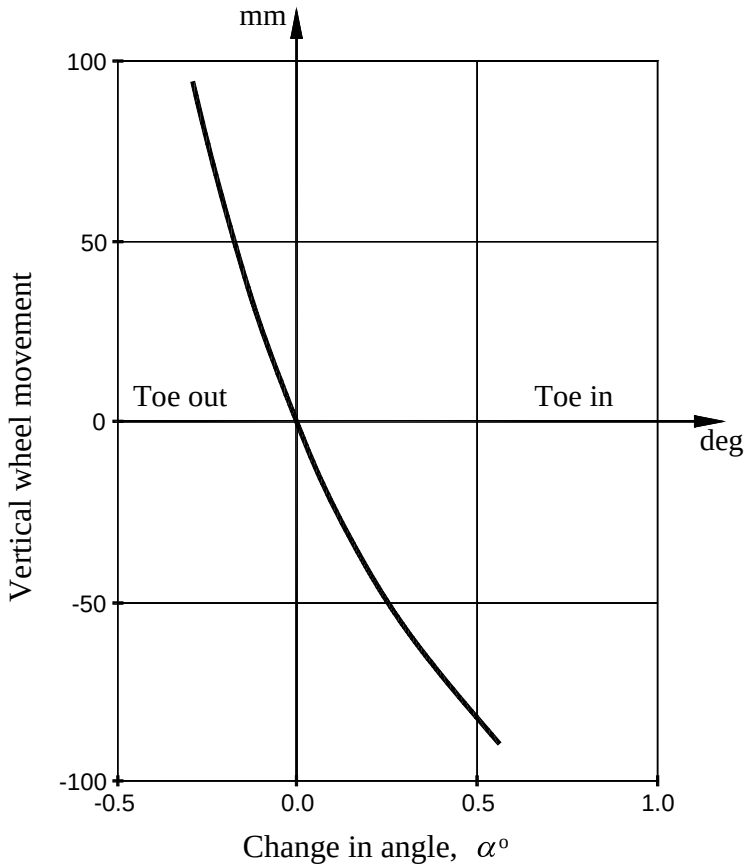

Figure 8.4-1 Toe-in change at jounce and rebound for a McPherson-suspension.

Due to the kinematics of the suspension, both wheels steer outward at cornering adding an understeer effect. It is customary to associate such an effect with the corresponding roll angle and let the ratio be the so called roll steer coefficient

$$\frac{\partial \delta}{\partial \phi}$$

where δ = induced steering angle
ϕ = roll angle

With the ISO-standard definition of positive angles it follows that

$$\frac{\partial \delta}{\partial \phi} \quad > \quad 0 \quad \rightarrow \text{överstyrning}$$
$$\frac{\partial \delta}{\partial \phi} \quad < \quad 0 \quad \rightarrow \text{understyrning}$$

for the front suspension.

Consider the vehicle in figure 8.4-1, with the front track width $t_{w12} = 1{,}45$ m. Then the roll steer coefficient can be estimated by approximating the curve with a straight line through the origin.

It then follows that

$$\frac{\partial \delta}{\partial \phi} = -\frac{0{,}2 \cdot \pi}{0{,}05 \cdot 180} \cdot \frac{1{,}45}{2} = -0{,}051$$

which is a realistic value.

8.4.1 Roll axle

Figure 8.4-2 shows a front double wishbone suspension, which at least used to be very common.

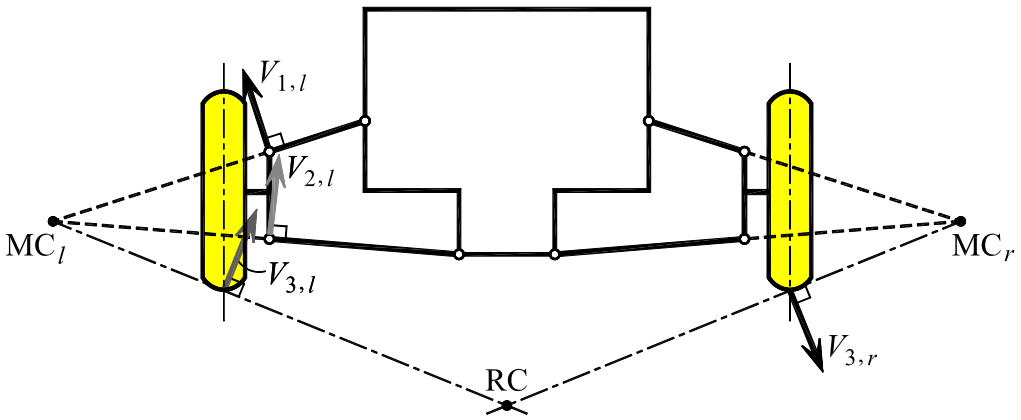

Figure 8.4-2 Positions of the instant centres of rotation of a double wishbone suspension. MC_L and MC_R are the instant centre of rotation of the left and right wheel respectively. RC is the instant centre of rotation of the sprung mass, the roll centre.

The motion of every body can be described by an instantaneous rotation around its *instant centre of rotation*. If the left wheel goes into jounce the motion can be described by a rotation around MC_L and the contact point of the wheel moves in the $v_{3,L}$ direction. Similarly, a rebound motion of the right wheel corresponds to a rotation around MC_R in the direction $v_{3,R}$.

Considering the roadway as a line between the contact points of the tyres, this corresponds to a rotation of the roadway clockwise around *RC* if the sprung mass is assumed to be fixed. If instead the roadway is fixed, RC is the point around which the sprung mass rotates. This point is usually called the roll centre. This can be constructed for both front- and rear suspension, and the imaginary line between these points is the roll axle. The sprung mass tends to rotate around this axis at cornering, and it is therefore important to be able to determine the roll stiffness for different suspensions to be able to determine load transfer at cornering. In figures 8.4-3 and 8.4-4 a number of different suspensions are analyzed and roll centres shown.

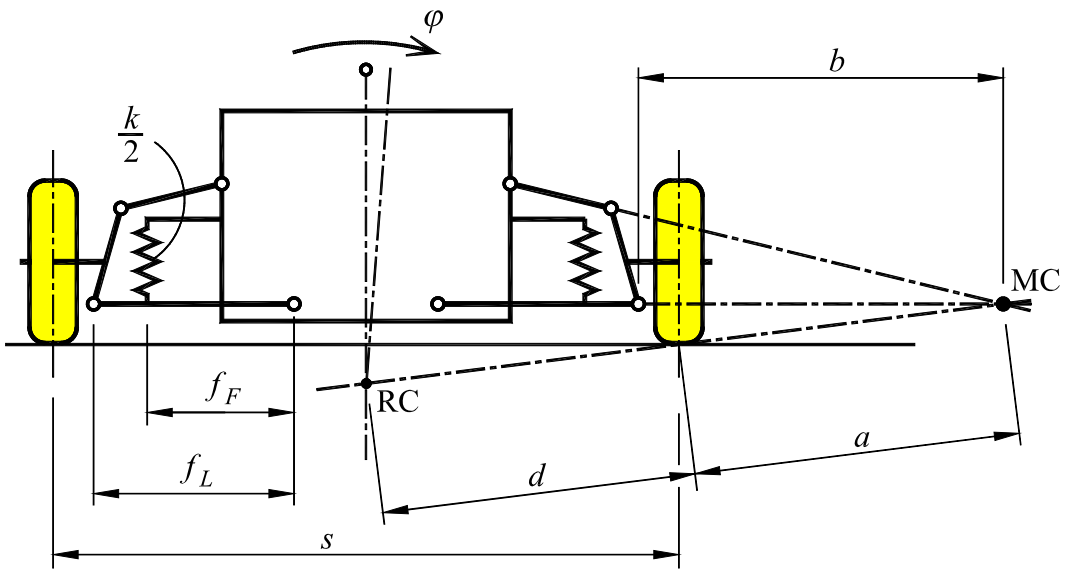

Figure 8.4-3a) Roll stiffness for double wishbone is given by: $\left(\frac{b \cdot d}{a}\right)^2 \cdot \left(\frac{f_F}{f_L}\right)^2 \cdot k$

where $\frac{k}{2}$ *is the spring constant for one spring.*

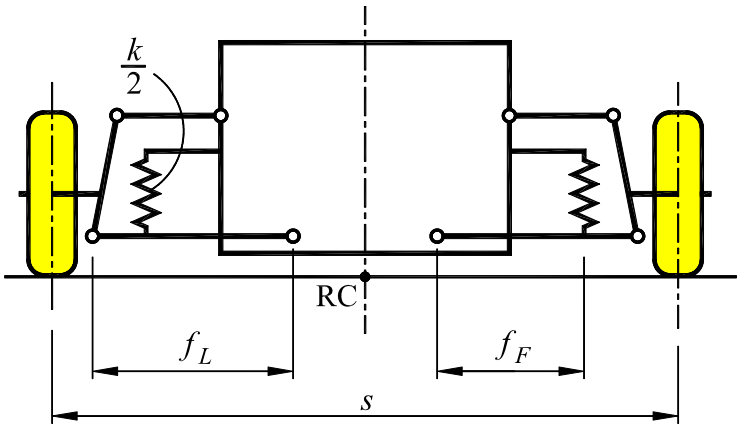

Figure 8.4-3b) The roll stiffness for a double wishbone suspension with parallel, horizontal arms is given by: $\left(\frac{s}{2}\right)^2 \cdot \left(\frac{f_F}{f_L}\right)^2 \cdot k$.

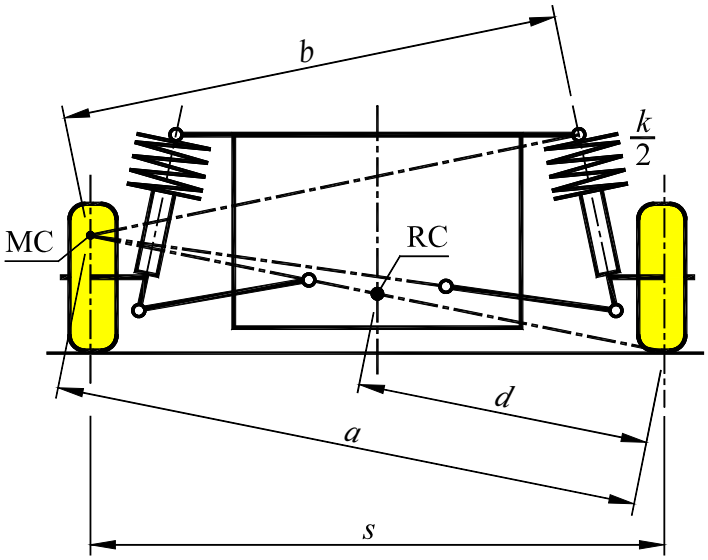

Figure 8.4-3c) Roll stiffness for McPherson suspension is given by: $\left(\frac{b \cdot d}{a}\right)^2 \cdot k$.

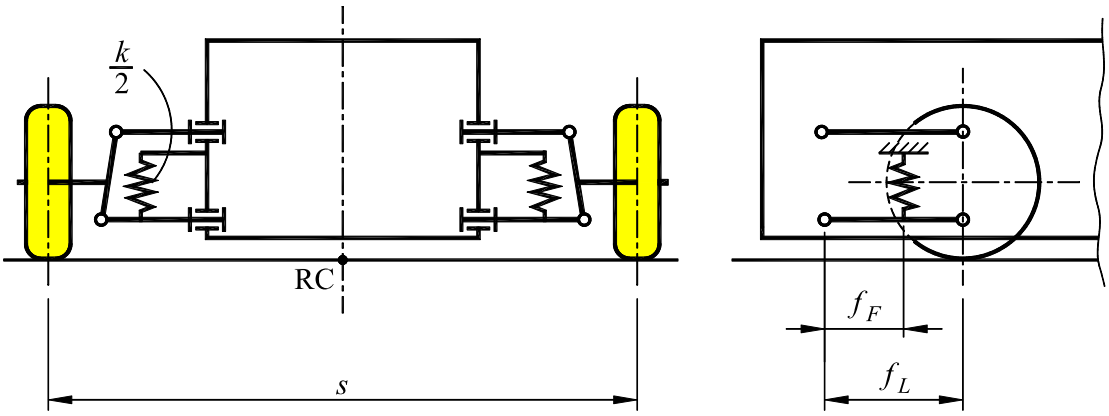

Figure 8.4-4a) Roll stiffness for double longitudinal swing arms is given by:

$$\left(\frac{s}{2}\right)^2 \cdot \left(\frac{f_F}{f_L}\right)^2 \cdot k \, .$$

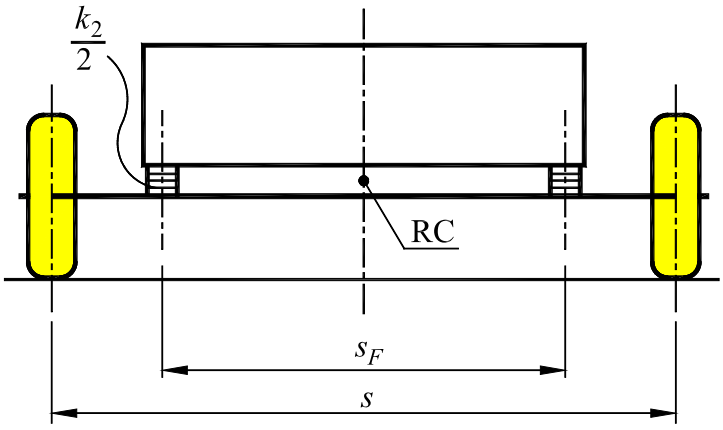

Figure 8.4-4b) Roll stiffness for rigid axle with leaf springs is given by: $\left(\frac{s_F}{2}\right)^2 \cdot k_2$.

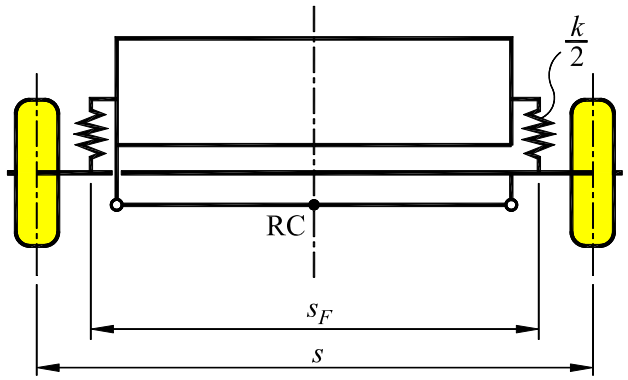

Figure 8.4-4c) Roll stiffness for rigid axle with panhard rod is given by: $\left(\frac{s_F}{2}\right)^2 \cdot k$.

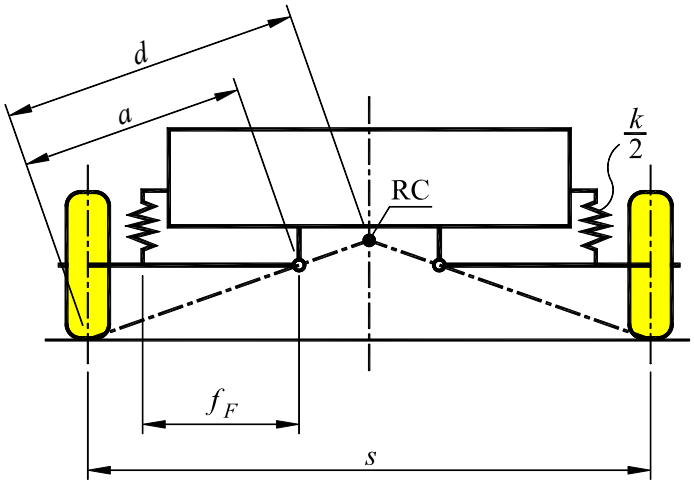

Figure 8.4-4d) Roll stiffness for swing axle is given by: $\left(\frac{f_F \cdot d}{a}\right)^2 \cdot k$

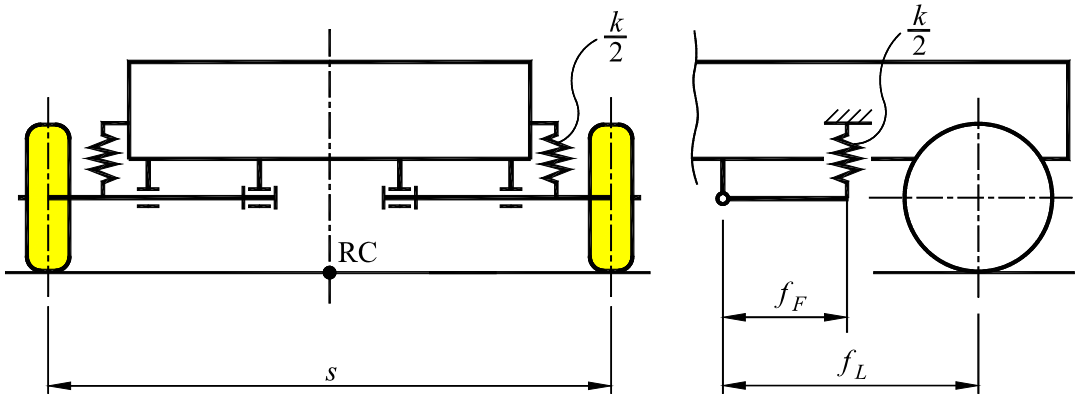

Figure 8.4-4e) Roll stiffness for backward pointing longitudinal swing arms is given by: $\left(\frac{s}{2}\right)^2 \cdot \left(\frac{f_F}{f_L}\right)^2 \cdot k$

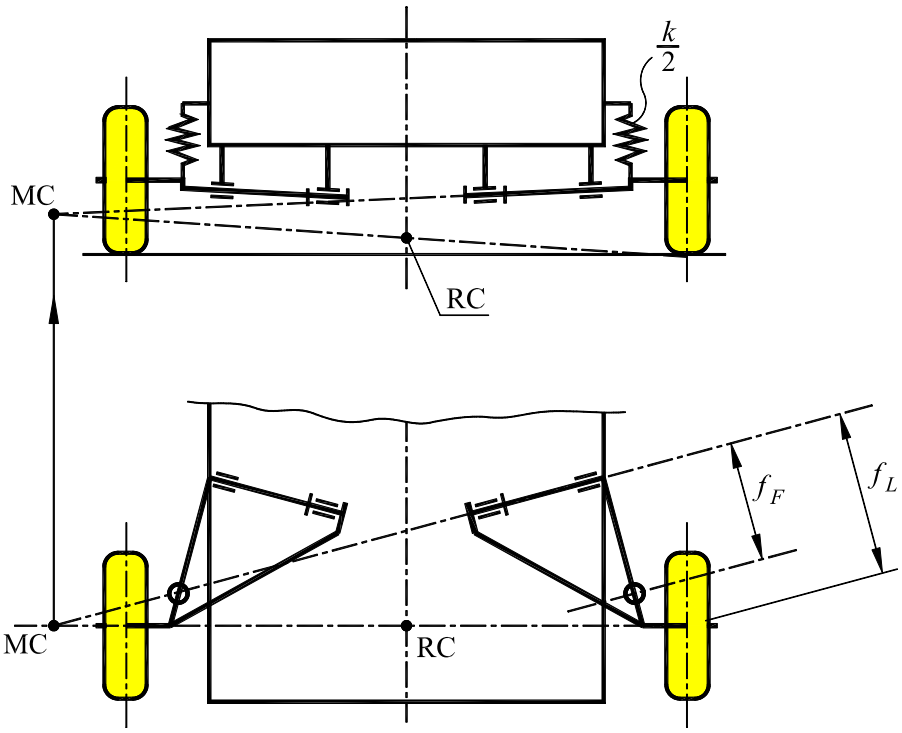

Figure 8.4-4f) Roll stiffness for inclined backward pointing swing arms is given by: $d^2 \cdot \left(\frac{f_F}{f_L}\right)^2 \cdot k$

In the following, the load transfer will be calculated at steady state cornering when taking into account the different roll stiffnesses. The unsprung masses will, however, be neglected, and the whole mass is assumed to lie in the sprung mass.

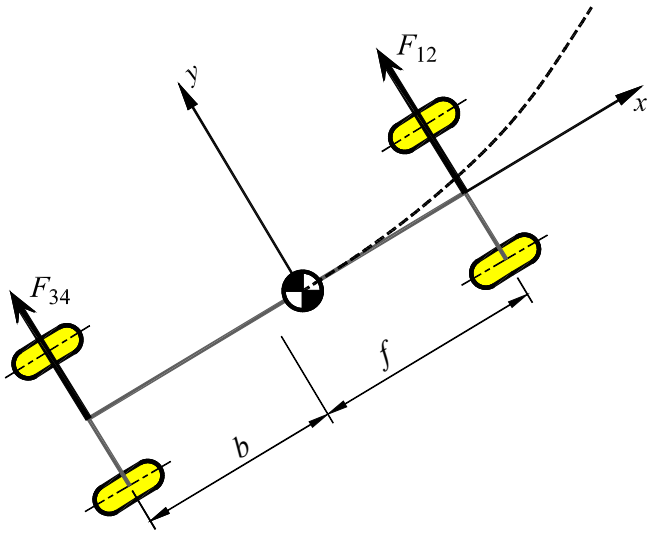

Figure 8.4-5 Lateral forces at steady state cornering.

Consider figure 8.4-5. If the lateral acceleration is denoted a_y, balance of forces at steady state requires that

$$m \cdot a_y = F_{12} + F_{34}$$

$$0 = f \cdot F_{12} - b \cdot F_{34}$$

It thus follows that

$$F_{12} = \frac{b}{L} \cdot m \cdot a_y \tag{8.4.1}$$

$$F_{34} = \frac{f}{L} \cdot m \cdot a_y \tag{8.4.2}$$

where

$$L = f + b$$

Force equilibrium for the sprung mass around the roll axis implies

$$0 = \left(C_F + C_B\right) \cdot \phi - m \cdot a_y \cdot h_e - m \cdot g \cdot h_e \cdot \phi$$

$$\phi = \frac{m \cdot h_e}{\left(C_F + C_B - m \cdot g \cdot h_e\right)} \cdot a_y \tag{8.4.3}$$

where

$$h_e = h - \frac{f \cdot e_b + b \cdot e_f}{L} \tag{8.4.4}$$

is the height of the centre of gravity above the roll axis (see figure 8.4-6).

Equation (8.4.3) gives the relation between lateral acceleration and roll angle, i.e.

$$\frac{\partial \phi}{\partial a_y} = \frac{m \cdot h_e}{\left(C_F + C_B - m \cdot g \cdot h_e\right)} \tag{8.4.5}$$

A couple of further relations are needed from equations (8.4.1) and (8.4.2):

$$\frac{\partial a_y}{\partial F_{12}} = \frac{L}{b \cdot m} \tag{8.4.6}$$

$$\frac{\partial a_y}{\partial F_{34}} = \frac{L}{f \cdot m} \tag{8.4.7}$$

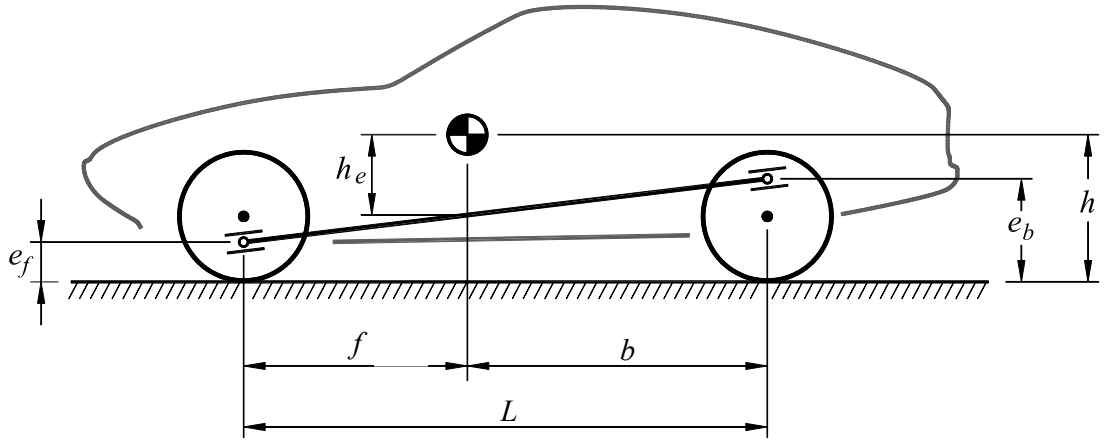

Figure 8.4-6 Roll axle position with related heights e_f and e_b.

The goal is to calculate the effective cornering stiffness when taking account of elasticities and kinematically induced steer angles. The strategy is to calculate the contribution to the steering angle for a given side force due to these effects, in the same manner as in section 8.3. The chain rule will thus be used several times. The (equivalent) contribution in steering angle due to camber follows from

$$\delta_\gamma = \delta_\gamma\left(\gamma\left(\phi\left(a_y\left(F_{12}\right)\right)\right)\right) \qquad => \qquad \frac{\partial \delta_\gamma}{\partial F_{12}} = \frac{\partial \delta_\gamma}{\partial \gamma} \cdot \frac{\partial \gamma}{\partial \phi} \cdot \frac{\partial \phi}{\partial a_y} \cdot \frac{\partial a_y}{\partial F_{12}}$$

Utilizing equations (8.2.2), (8.4.5) and (8.4.6) this can be rewritten as

$$\frac{\partial \delta_\gamma}{\partial F_{12}} = -\frac{C_\gamma}{C_\alpha} \cdot \frac{\partial \gamma}{\partial \phi} \cdot \frac{m \cdot h_e}{C_{TOT}} \cdot \frac{L}{b \cdot m} = -\frac{C_\gamma}{C_\alpha} \cdot \frac{\partial \gamma}{\partial \phi} \cdot \frac{h_e}{C_{TOT}} \cdot \frac{L}{b} \tag{8.4.8}$$

where

$$C_{TOT} = C_F + C_B - m \cdot g \cdot h_e \tag{8.4.9}$$

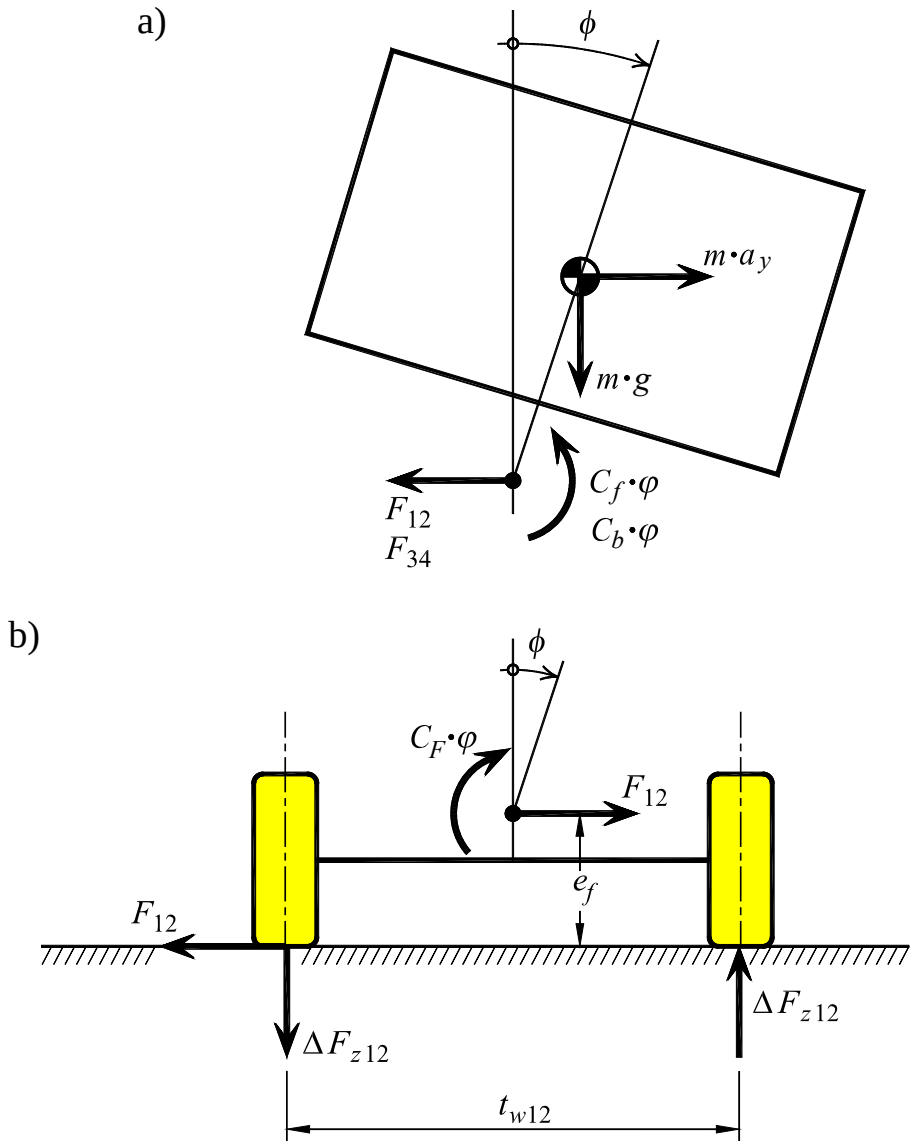

Figure 8.4-7 Forces and moments between sprung and unsprung mass. Only front axle shown.

Roll steer is handled the same way as the camber force contribution to the steering angle outlined above

$$\delta_\phi = \delta_\phi\left(\phi\left(a_y(F_{12})\right)\right)$$

$$\frac{\partial \delta_\phi}{\partial F_{12}} = \frac{\partial \delta_\phi}{\partial \phi} \cdot \frac{\partial \phi}{\partial a_y} \cdot \frac{\partial a_y}{\partial F_{12}} = \frac{\partial \delta_\phi}{\partial \phi} \cdot \frac{h_e}{C_{TOT}} \cdot \frac{L}{b} \qquad (8.4.10)$$

The corresponding effect for the interaction of the wheels with elasticities in the steering system and suspension has already been calculated. In analogy with equation (8.3.4) the contributions to the steering angle from the respective effect are added:

$$\alpha_V = \alpha + \delta_{su} + \delta_s^{'} + \delta_\gamma + \delta_\phi$$

However,

$$\alpha_V = -\frac{F_{12}}{C_{12}} \quad ; \quad \alpha = -\frac{F_{12}}{2 \cdot C_\alpha}$$

and

$$\delta_{su} = -\frac{(n_{su} - t_0) \cdot F_{12}}{2 \cdot C_{su}} \quad ; \quad \delta_s' = -\frac{(n_c - t_0) \cdot F_{12}}{C_s'}$$

$$\delta_\gamma = \frac{\partial \delta_\gamma}{\partial F_{12}} \cdot F_{12} \quad ; \quad \delta_\phi = \frac{\partial \delta_\phi}{\partial F_{12}} \cdot F_{12} \tag{8.4.11}$$

It thus follows that

tyres — suspension elasticity — steering elasticity

$$\frac{1}{C_{12}} = \frac{1}{2 \cdot C_\alpha} + \frac{(n_{su} - t_0)}{2 \cdot C_{su}} + \frac{(n_c - t_0)}{C_s'} + \frac{C_\gamma}{C_\alpha} \cdot \frac{\partial \gamma}{\partial \phi} \cdot \frac{h_e}{C_{TOT}} \cdot \frac{L}{b} - \frac{\partial \delta_\phi}{\partial \phi} \cdot \frac{h_e}{C_{TOT}} \cdot \frac{L}{b} \tag{8.4.12}$$

camber effect — roll steer

Table 8.4-1 A set of realistic values for a car.

Symbol	Value	Unit	Symbol	Value	Unit
$2 \cdot C_\alpha$	80000	N/rad	h	0,55	M
t_0	-0,05	M	e_f	0,03	M
n_{su}	0,05	M	e_b	0,30	M
C_{su}	40000	Nm/rad	L	2,76	M
n_c	0,02	M	f	1,20	M
C_s'	25000	Nm/rad	b	1,56	M
C_γ	2000	N/rad	C_F	30000	Nm/rad
m	1400	Kg	C_B	20000	Nm/rad
$\frac{\partial \gamma}{\partial \phi}$	0,9	(front)	$\frac{\partial \delta_\phi}{\delta \phi}$	-0,05	(front)

Insertion of these values gives the following result

$$\frac{1}{C_{12eff}} = 10^{-4}\left(\frac{1}{8}+\frac{1}{80}+\frac{1}{36}+\frac{1}{153}+\frac{1}{137}\right) = \frac{1}{56000}$$

with the terms in the same order as in equation (8.4.12). The cornering stiffness has thus been reduced from 80000 N/rad (tyres only) to 56000 N/rad with all effects included. In this case, the order of significance is

1. Steering elasticity
2. Suspension elasticity
3. Roll steer
4. Camber due to roll

There are naturally additional effects which influence the effective cornering stiffness. An applied side force can also change the camber angle because of bushings in the suspension.

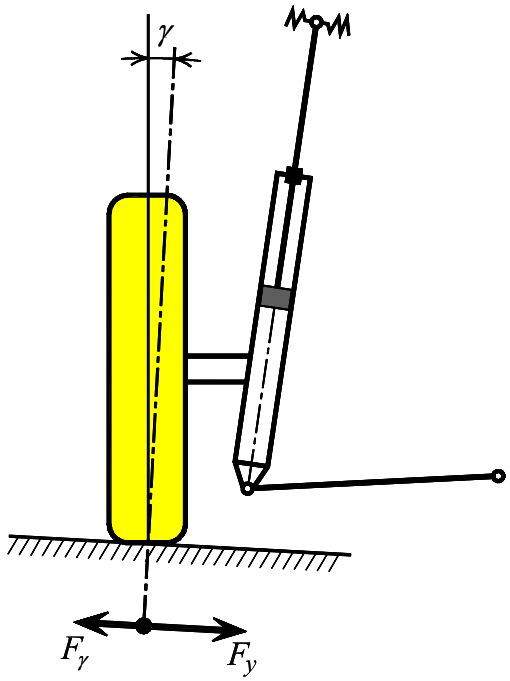

Figure 8.4-8 Effect on camber angle due to side force.

For a McPherson suspension a normal value is

$$\frac{\partial\gamma}{\partial F_y} = 0{,}33°/kN \quad \text{per wheel} \qquad (8.4.13)$$

This effect on the cornering stiffness will in the following be calculated. In figure 8.4-8 the total side force F_{ytot} is composed of the tyre force F_y due to the slip angle α, and the camber force F_γ:

$$F_{ytot} = F_y + F_\gamma$$

Due to the side force the upper attachment point (a bushing) will be displaced, and cause an increase in the camber angle γ

$$\gamma = \frac{\partial\gamma}{\partial F_y}\cdot F_{ytot}$$

The camber force can be expressed as $F_\gamma = -C_\gamma \cdot \gamma = -C_\gamma \dfrac{\partial\gamma}{\partial F_y}\cdot F_{ytot}$

and thus

$$F_{ytot} = \frac{F_y}{1 + C_\gamma \cdot \frac{\partial \gamma}{\partial F_y}}$$

For small slip angles this implies a reduction of the cornering stiffness through

$$C_{\alpha eff} = \frac{C_\alpha}{1 + C_\gamma \cdot \frac{\partial \gamma}{\partial F_y}}$$

With equation (8.4.13) and values from table 8.4-1 it can be concluded that the reduction is around 3 to 4% which is slightly smaller than the other effects.

It is important to note that equation (8.4.12) is only valid at steady-state, with fully developed roll angle (camber effect and roll steer). For transient manoeuvres, the effect of the elasticities dominates.

8.5 The side force dependence on normal force

The reasoning in the previous section is based on linearizations, and is in principle applicable only for small input signals, i.e. small steering wheel angles, and thus small lateral accelerations and yaw angle velocities. The previously described effects naturally have significance also for higher lateral accelerations; however, there are additional effects due to the nonlinear characteristics of tyres. Particularly, in this section the effect of the normal force is studied.

For this reason the first aim is to calculate the load transfer at cornering for an axle according to figure 8.4-7. The moment equilibrium about the point in the ground plane directly below the roll axle at the front axle is

$$F_{12}\ e_f + C_f\ \phi = \Delta F_{z12} \cdot t_{w12}$$

and by substitution of equations (8.4.1) and (8.4.3) the change in normal force is thus

$$\Delta F_{z12} = \frac{1}{t_{w12}} \left(\frac{b}{L} m e_f + \frac{m h_e C_f}{C_f + C_b - m g h_e} \right) a_y \qquad (8.5.1)$$

In similar fashion, it follows that the change in formal force for the rear tyres are

$$\Delta F_{z34} = \frac{1}{t_{w34}} \left(\frac{f}{L} m e_b + \frac{m h_e C_b}{C_f + C_b - m g h_e} \right) a_y \qquad (8.5.2)$$

For a designer of wheel suspensions there are two parameters which can be chosen more or less independently; the *roll stiffnesses* $C_{f,b}$ and the *roll axle heights* $e_{f,b}$. This

provides an opportunity to control the distribution of load transfer between front and rear axles.

At cornering, there is a load transfer from the curve-inner to the curve-outer wheels. By having different roll stiffnesses and/or different roll axle heights for front and rear axis, the load transfer can be different for the respective axles. An axle with high roll stiffness has a large amount of load transfer and an axle with low roll stiffness has a small amount of load transfer. To increase the roll stiffness, so called torsion bars can be mounted, which usually consist of torsion springs. See figure 8.5.1.

The load transfer is of considerable importance because of the nonlinear properties of tyres, both with regard to the *cornering stiffness* and the maximum achievable *friction coefficient*. Consider for example figure 8.5-2 where the cornering stiffness, C_α, is plotted as a function of the vertical load, F_z, for a Michelin ZX 155 SR 14 tyre.

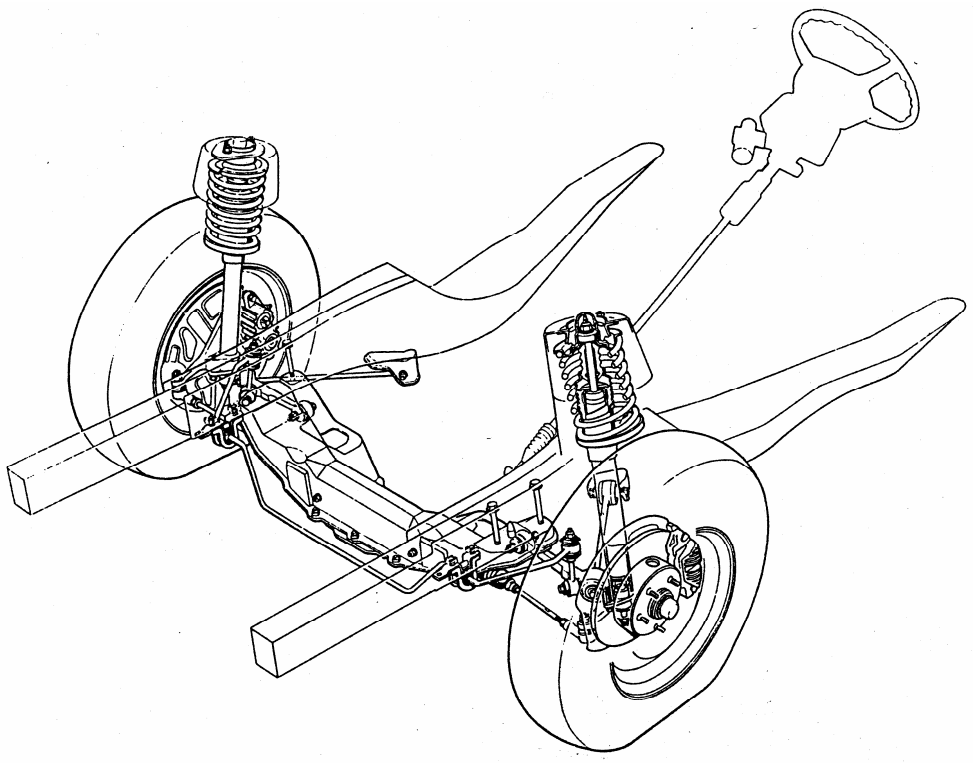

Figure 8.5-1 McPherson-suspension with torsion bar.

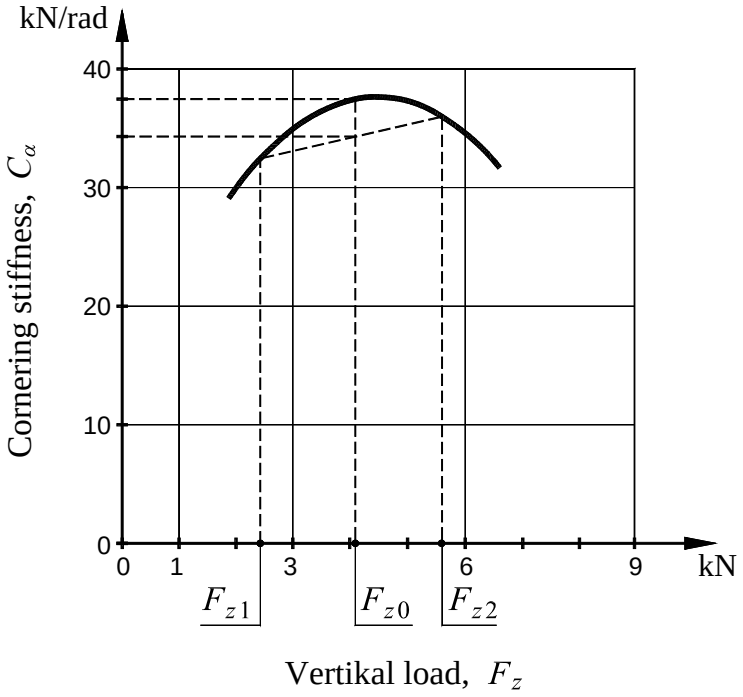

Figure 8.5-2 Cornering stiffness, C_α, as a function of vertical load, F_z. Michelin ZX 155 SR 14. F_{z0} is vertical load at equal tyre load. F_{z1} and F_{z2} corresponds to a load transfer of 1500 N.

Since the relationship between the cornering stiffness C_α and the vertical load F_z is a concave curve (see figure 8.5-2) it follows that

$$C_\alpha(F_{z0}) \geq \frac{C_\alpha(F_{z1}) + C_\alpha(F_{z2})}{2}$$

where

$$F_{z0} = \frac{F_{z1} + F_{z2}}{2}$$

This means that at a load transfer of 1500 N the reduction in the resultant cornering stiffness is about 10%. The same reasoning can be used for the maximum side force. First, consider the dependence of the maximum friction coefficient, μ_y, on the vertical load. In figure 8.5-3 it can be seen that the friction *decreases* with increasing load. It can therefore be concluded that a car with most of the weight on the front axle (which typically is the case) will loose traction on this axle first.

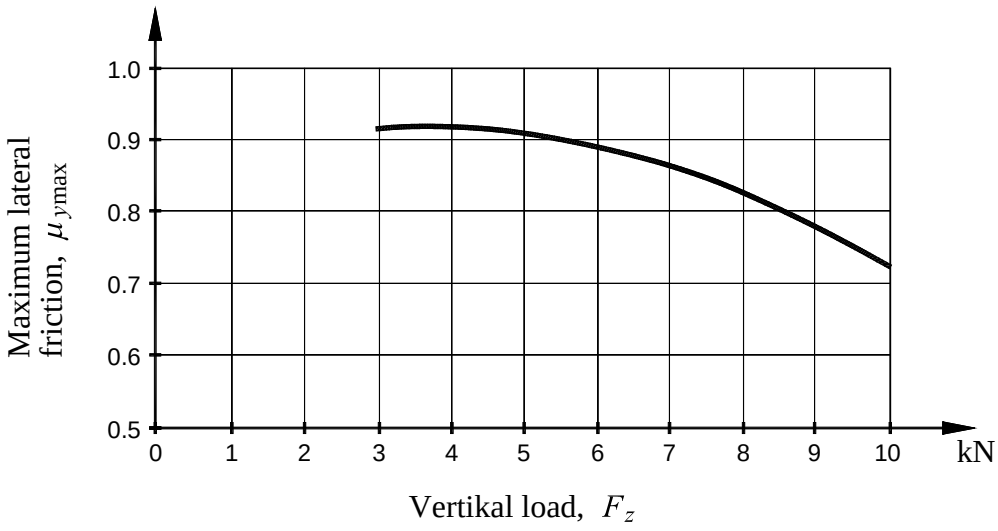

Figure 8.5-3 Maximum friction coefficient, μ_y, as a function of vertical load, F_z.

Semperit 185 SR 14 tyre.

This effect can in some cases be amplified further by the load transfer. If the function in figure 8.5-3 is multiplied by F_z the result is a diagram of the maximum lateral force as a function of vertical load, and this function is sometimes *concave* like the cornering stiffness in figure 8.5-2, and the exact same reasoning about load transfer can then be made. See the example in figure 8.5-4.

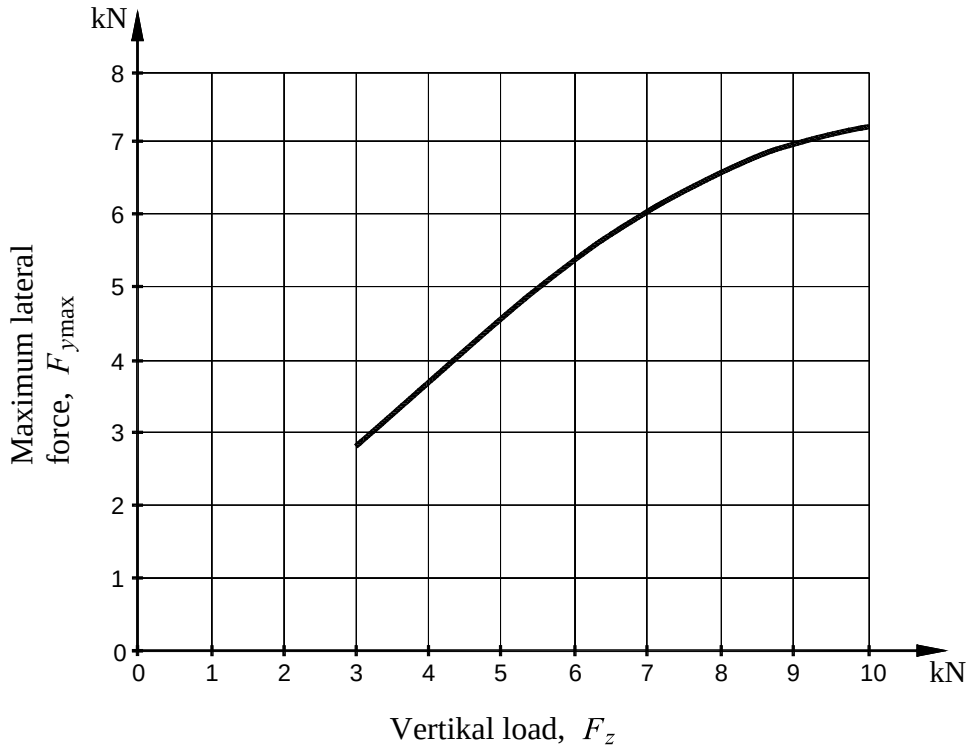

Figure 8.5-4 Maximum lateral force, F_y, as a function of vertical load, F_z.

Semperit 185 SR 14 tyre.

The same reasoning can also be made of intermediate slip angles. In figure 8.5-5 the lateral force as a function of vertical load is plotted for two different slip angles, 2 and 5 degrees. Both curves are concave and in analogy with the previous cases a load transfer results in a reduction in the resultant lateral force.

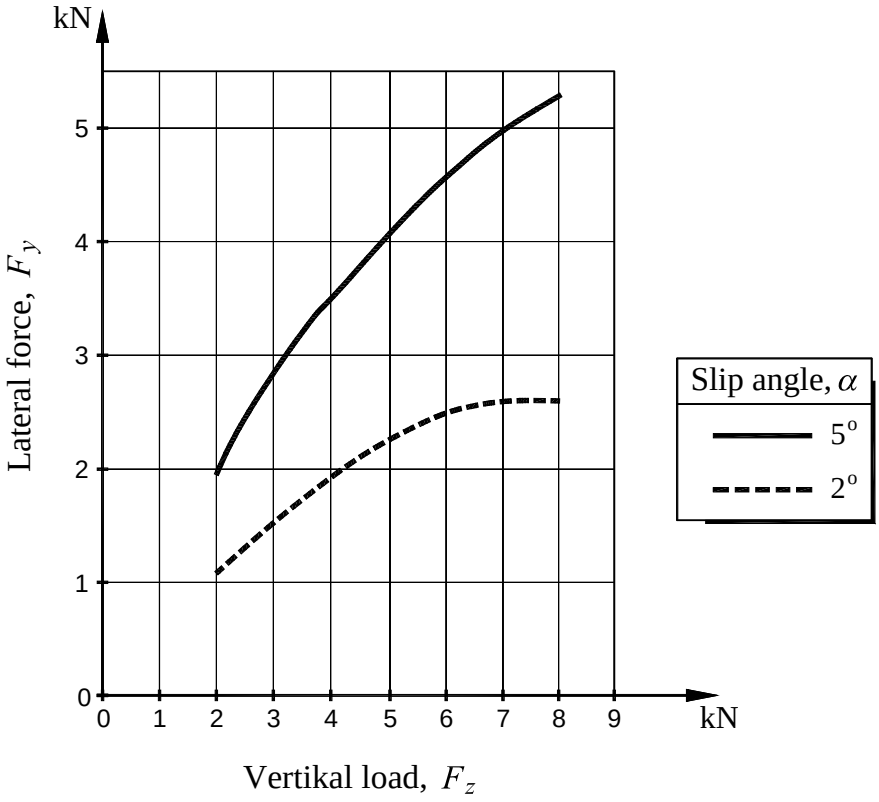

Figure 8.5-5 Lateral force, F_y, as a function of vertical load, F_z, for slip angles of 2 and 5 degrees. Tyres 195/60 HR 14.

It must be emphasized that the degree of nonlinearity varies between different manufacturers and tyre models. The phenomena described above can thus be more or less prominent for other type of tyres, however, the tendencies are usually similar. The driving characteristics of a car can therefore be changed just by switching manufacturer of the tyres.

In summary, if the majority of the weight is on the front axle, traction is lost at the front tyres first, i.e. the car understeers at the limit. Additionally, if the majority of the load transfer occurs on the front axle, this also contributes in the understeer direction.

8.6 Handling diagram

In section 8.3 it was shown how the effective cornering stiffness is changed when the suspension contains elastic elements like rubber bushings. This analysis can naturally be generalized to all slip angles, and not just to the linear neighbourhood of the origin. As an example, assume that tyre and suspension characteristics according to figure 8.6-1 has been measured.

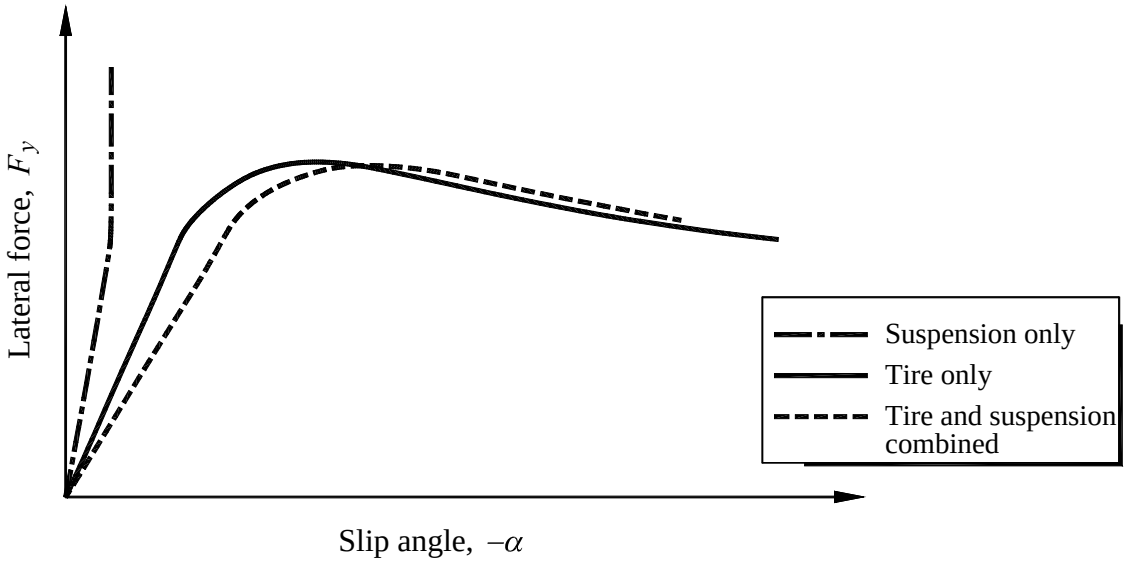

Figure 8.6-1 Construction of the resulting characteristic.

This case corresponds to figure 8.3-1 with $t_0 < n_{su}$, i.e. the pivot point is *in front* of the acting point of the tyre's side force.

The actual suspension is assumed to yield, or flex, according to the same figure. The resulting characteristic is obtained by adding the slip angle and the steer angle for the same lateral force. In this manner the previously described effects can be included, and the effective side force characteristic for the front and rear axle can be calculated even for high slip angles. The goal is to derive relations and diagrams which are valid even in the nonlinear region and not just for small lateral forces.

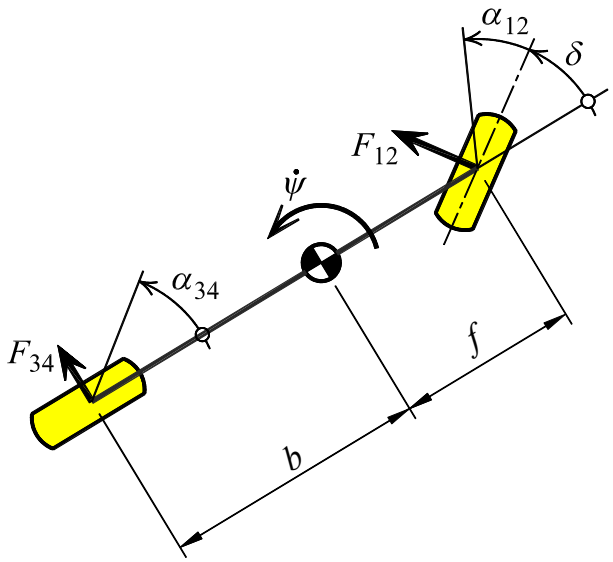

Figure 8.6-2 Positive directions for steer and slip angles.

In steady-state it follows for the vehicle in figure 8.6-2 that:

$$\begin{cases} m \cdot a_y = F_{12} + F_{34} \\ 0 = f \cdot F_{12} - b \cdot F_{34} \end{cases} \qquad (8.6.1)$$

$$\begin{cases} \alpha_{12} = \dfrac{v_y + f \cdot \dot{\Psi}}{v_x} - \delta \\ \alpha_{34} = \dfrac{v_y - b \cdot \dot{\Psi}}{v_x} \end{cases} \qquad (8.6.2)$$

Equation (8.6.1), with $f + b = L$, then yields

$$m \cdot a_y = F_{12} \cdot \frac{L}{b} \qquad (8.6.3)$$

$$m \cdot a_y = F_{34} \cdot \frac{L}{f}$$

Introducing the axle loads

$$\begin{cases} F_{z12} = \dfrac{b}{L} \cdot m \cdot g \\ F_{z34} = \dfrac{f}{L} \cdot m \cdot g \end{cases}$$

makes it possible to express equation (8.6.3.) as

$$\frac{F_{12}}{F_{z12}} = \frac{F_{34}}{F_{z34}} = \frac{a_y}{g} \qquad (8.6.4)$$

Equation (8.6.2) gives with $L = f + b$

$$\alpha_{34} - \alpha_{12} = \delta - \frac{L}{v_x} \cdot \dot{\psi} = \delta - \frac{L}{R} \qquad (8.6.5)$$

where R denotes the curve radius of the circular driving.

Equation (8.6.4) gives a relation between the normalized tyre forces (friction utilization) and the lateral acceleration of the vehicle. As previously, it is possible to construct the side force characteristics for front and rear axle and normalize these by dividing with the respective normal force.

$$\mu_{12} = \mu_{12}(-\alpha_{12}) = \frac{F_{12}(-\alpha_{12})}{F_{z12}} = \frac{a_y}{g}$$

$$\mu_{34} = \mu_{34}(-\alpha_{34}) = \frac{F_{34}(-\alpha_{34})}{F_{z34}} = \frac{a_y}{g}$$

Both of them could for example look like in figure 8.6-3.

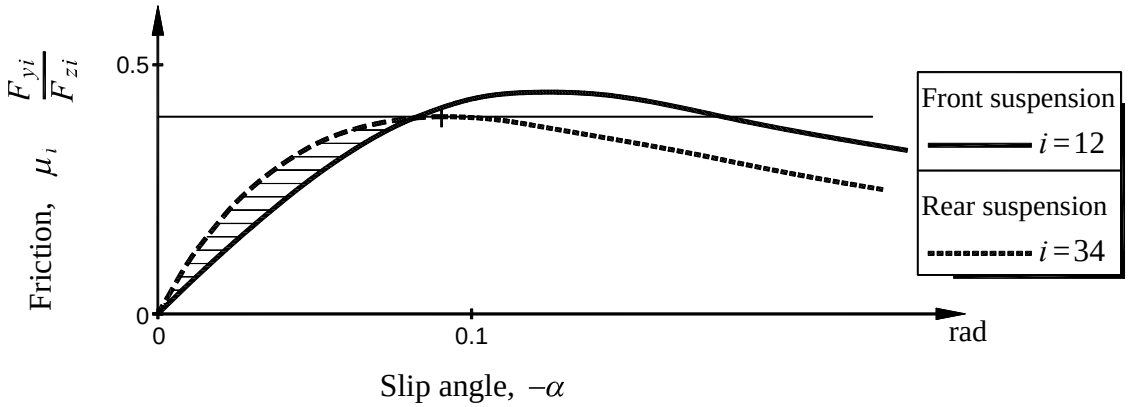

Figure 8.6-3 Examples of two normalized axle characteristics.

According to equation (8.6.4) it is then possible to find the slip angles α_{12} and α_{34} which correspond to a given lateral acceleration a_y. Equation (8.6.5), on the other hand, relates the difference in slip angles to the steer angle δ.

For every value of a_y/g the μ-curves are subtracted from each other according to

$$-\alpha_{12} = \mu_{12}^{-1}\left(\frac{a_y}{g}\right)$$

$$-\alpha_{34} = \mu_{34}^{-1}\left(\frac{a_y}{g}\right)$$

$$\alpha_{34} - \alpha_{12} = \mu_{12}^{-1}\left(\frac{a_y}{g}\right) - \mu_{34}^{-1}\left(\frac{a_y}{g}\right)$$

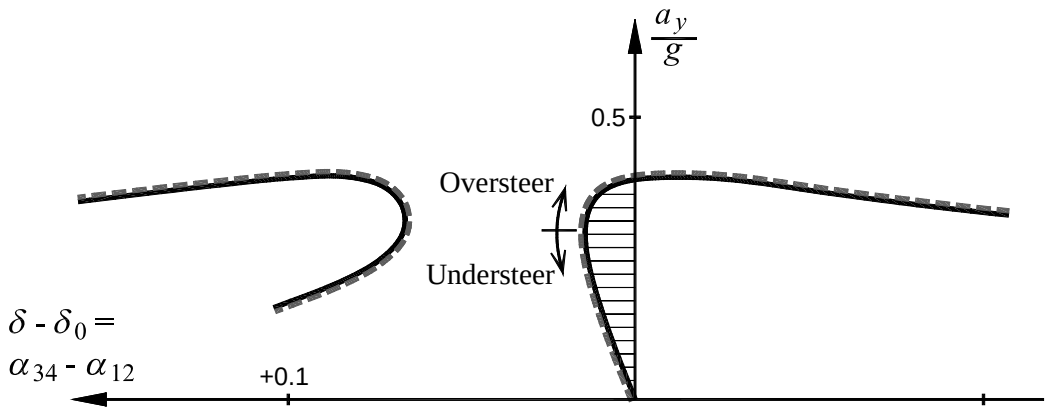

Figure 8.6-4 Handling diagram. Slip angle difference $\alpha_{12} - \alpha_{34}$ as a function of a_y/g. Axle characteristics according to figure 8.6-3. The right curve is the main branch with $-\alpha_{12} < 0.1$ rad.

The resulting handling diagram in figure 8.6-4 should be related to the steer angle δ and circle radius R by equation (8.6.5).

First, consider the simple relation that the centripetal acceleration is equal to the lateral acceleration of the vehicle:

$$a_y = \frac{v_x^2}{R}$$

i.e.

$$\frac{a_y}{g} = \frac{v_x^2}{L \cdot g} \cdot \frac{L}{R}$$

The linear relation between a_y/g and L/R is plotted in figure 8.6-5. The slope of lines are v_x^2 / Lg.

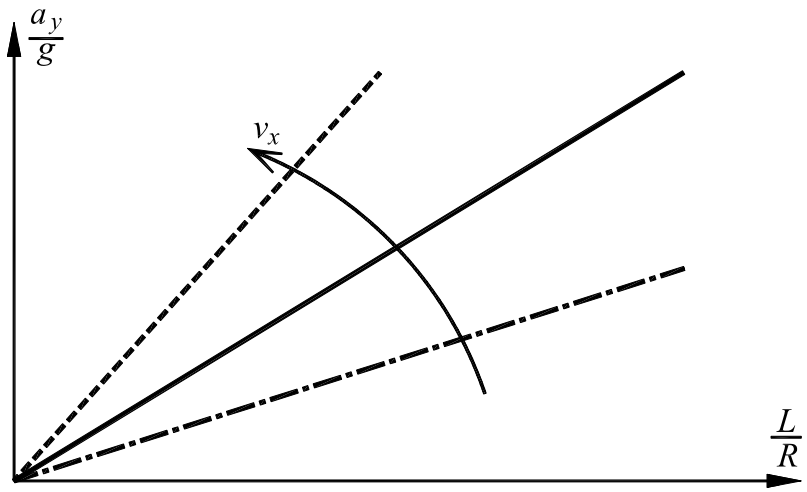

Figure 8.6-5 Relation between lateral acceleration and curvature.

The diagram in figure 8.6-5 can be related to the diagram in figure 8.6-4. By using equation (8.6.5) it follows that

$$\delta = \alpha_{34} - \alpha_{12} + \frac{L}{R} = \alpha_{34} - \alpha_{12} + \delta_0$$

which gives a relation between the diagrams. See the illustration in figure 8.6-6.

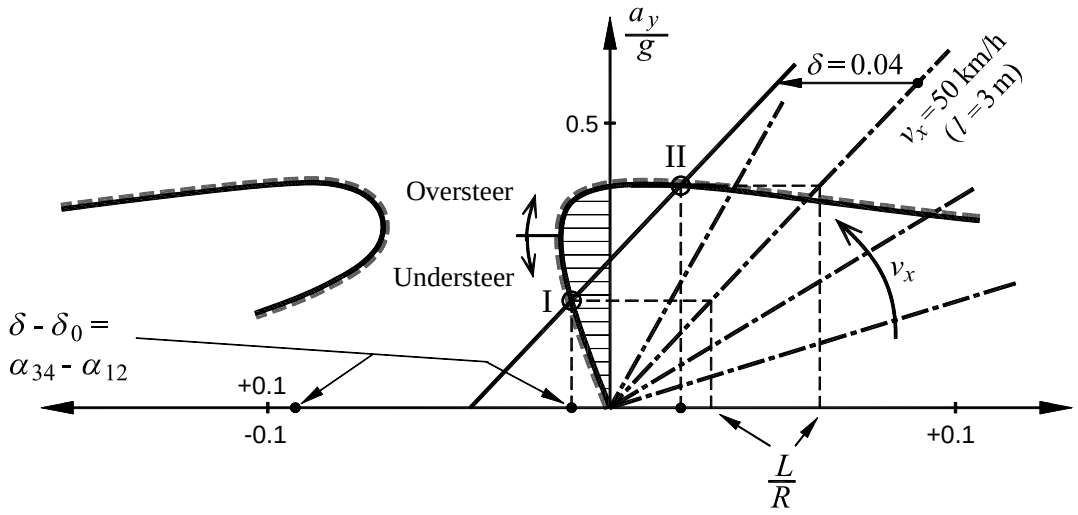

Figure 8.6-6 Handling diagram from normalized axle characteristics in figure 8.6-3. With the speed 50 km/h and radius R = 150 m (L/R = 0,02) the steer angle is δ = 0,04 rad. ≈ 2,3°.

The data for handling diagrams is possible to collect at field tests. It is only necessary to measure the steering wheel angle at different speeds for a given circular path. A couple of examples are shown in figures 8.6-7 to 8.6-10.

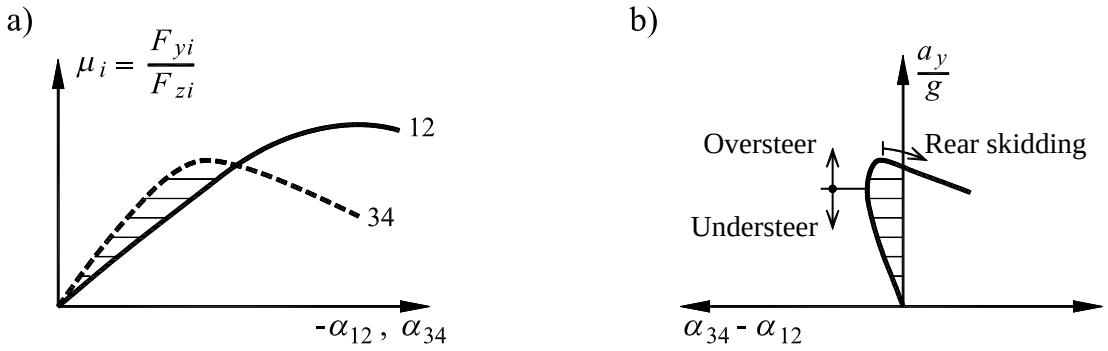

Figure 8.6-7 Handling diagram for a vehicle which understeer at small slip angles and oversteer at high slip angles. Only the main branch is plotted.

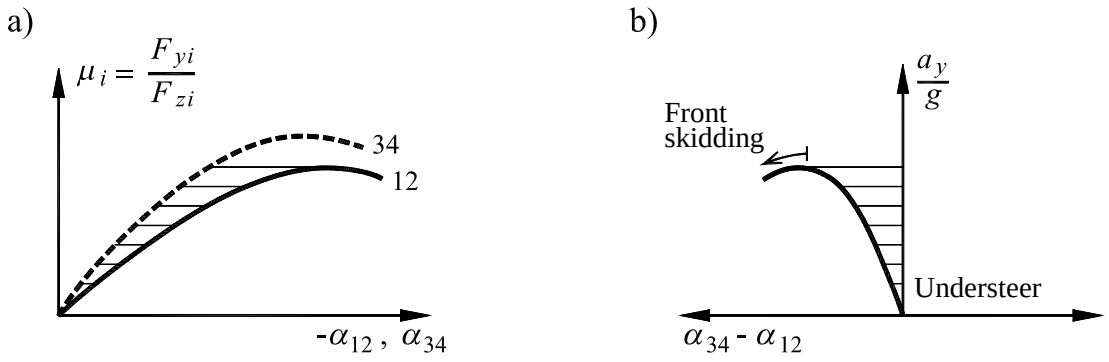

Figure 8.6-8 Handling diagram for a vehicle which understeer. Only the main branch is plotted.

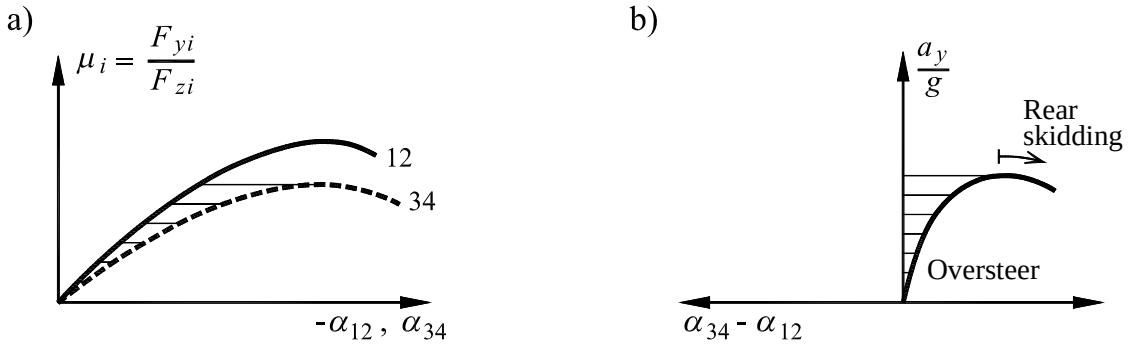

Figure 8.6-9 Handling diagram for a vehicle which oversteer. Only the main branch is plotted.

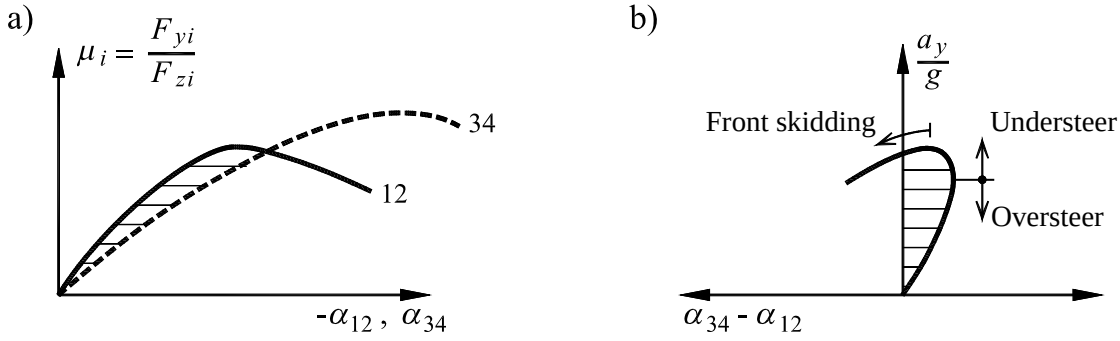

Figure 8.6-10 Handling diagram for a vehicle which oversteer for small slip angles and understeer for high slip angles. Only the main branch is plotted.